The Journal of Chemical Physics ARTICLE scitation.org/journal/jcp

Ab initio molecular dynamics with screened Lorentz forces. I. Calculation and atomic charge interpretation of Berry curvature

Cite as: J. Chem. Phys. 155, 024104 (2021); doi: 10.1063/5.0055388
Submitted: 28 April 2021 • Accepted: 7 June 2021 •
Published Online: 8 July 2021

Tanner Culpitt, Laurens D. M. Peters, Erik I. Tellgren,[a] and Trygve Helgaker

AFFILIATIONS

Hylleraas Centre for Quantum Molecular Sciences, Department of Chemistry, University of Oslo, P.O. Box 1033 Blindern, N-0315 Oslo, Norway

[a]Author to whom correspondence should be addressed: erik.tellgren@kjemi.uio.no

ABSTRACT

The dynamics of a molecule in a magnetic field is significantly different from its zero-field counterpart. One important difference in the presence of a field is the Lorentz force acting on the nuclei, which can be decomposed as the sum of the bare nuclear Lorentz force and a screening force due to the electrons. This screening force is calculated from the Berry curvature and can change the dynamics qualitatively. It is therefore important to include the contributions from the Berry curvature in molecular dynamics simulations in a magnetic field. In this work, we present a scheme for calculating the Berry curvature numerically using a finite-difference technique, addressing challenges related to the arbitrary global phase of the wave function. The Berry curvature is calculated as a function of bond distance for H_2 at the restricted and unrestricted Hartree–Fock levels of theory and for CH^+ as a function of the magnetic field strength at the restricted Hartree–Fock level of theory. The calculations are carried out using basis sets of contracted Gaussian functions equipped with London phase factors (London orbitals) to ensure gauge-origin invariance. In this paper, we also interpret the Berry curvature in terms of atomic charges and discuss its convergence in basis sets with and without London phase factors. The calculation of the Berry curvature allows for its inclusion in *ab initio* molecular dynamics simulations in a magnetic field.

I. INTRODUCTION

In quantum chemistry and quantum mechanics more generally, the Berry phase[1–5] and Berry curvature[2] are prevalent and important concepts, particularly when dealing with molecular dynamics in magnetic fields. For the purposes of this work, we are interested in how the Berry curvature manifests itself in molecular dynamics equations. We concern ourselves here with Born–Oppenheimer molecular dynamics (BOMD),[6,7] which is predicated upon the Born–Oppenheimer approximation[8] where the electrons of an atomic or molecular system are assumed to respond instantaneously to any perturbations in nuclear coordinates. The total approximate ground-state wave function is thereby written as a product of the electronic and nuclear wave functions, although, in principle, the exact wave function can also be represented in product form.[9–11] When formulating BOMD in the absence of fields, where the electronic wave function can be taken as real, the nuclear Hamiltonian can be approximated by the sum of the nuclear kinetic energy and a scalar potential. In this setting, the equations of motion for the nuclei reduce to Newton's equations, with the conservative force on each nucleus calculated as the negative gradient of the electronic potential-energy surface.

For BOMD in a magnetic field, the situation is more complicated because of the velocity-dependent forces. The electronic wave function is generally complex, and the nuclear Born–Oppenheimer Hamiltonian contains contributions from both magnetic and geometric vector potentials. The magnetic vector potential gives rise to the bare Lorentz force acting on the nuclei, while the geometric vector potential gives rise to the Berry force, representing the effect of the screening of the magnetic field by the electrons in the system.[2,12–14] The total effective Lorentz force acting on the nuclei is the sum of the bare Lorentz force and the Berry screening force. The screening force can be large and change the dynamics qualitatively, making its implementation an important step toward a full

realization of BOMD in a magnetic field, as described in a companion article to the present paper.

The present work takes a direct, finite difference approach to the Berry curvature. The main challenge associated with calculating the Berry curvature in this way is that the global phase of the wave function for each nuclear perturbation is, in principle, arbitrary. It is therefore important to have a consistent, well-justified way of dealing with the phase. Previously, Ceresoli, Marchetti, and Tosatti have obtained the Berry force from the Berry curvature for H_2 using a simple model electronic wave function.[12] Here, we present a general finite-difference implementation of the Berry curvature within the software package LONDON for *ab initio* molecular electronic-structure calculations in a finite magnetic field.[15] The LONDON program uses London atomic orbitals [also known as gauge-including atomic orbitals (GIAOs)][16–23] for the gauge-origin invariant calculation of energies and molecular properties at various levels of theory including Hartree–Fock theory,[20,21,24] (current-) density functional theory,[25,26] full-configuration-interaction theory,[27,28] coupled-cluster theory,[29] and linear-response theory.[30]

This work is organized as follows: Section II contains a derivation of the effective nuclear Hamiltonian in the presence of a magnetic field, along with the resulting equations of motion and the finite difference scheme for the calculation of the Berry curvature. Justification for the phase corrections used to account for the arbitrary phase of the electronic wave function is also presented. Section III presents Berry curvature results for H_2 and CH^+ at the Hartree–Fock level of theory. For H_2, comparisons are made with the previous results of Ref. 12. Summary and future directions are given in Section IV.

II. THEORY

We consider a joint system of nuclei and electrons. Throughout this work, I and J serve as indices for the N_{nuc} nuclei, and their lowercase counterparts i and j will serve as indices for the N_{el} electrons. We use the notations M_I, Z_I, and $\mathbf{R}_I$ for the mass, atom number, and position of nucleus I, respectively. We use $\mathbf{r}_i$ and $\mathbf{p}_i$ for the position operator and momentum operator of electron i, respectively. The vectors of collective nuclear and electronic coordinates are denoted by $\mathbf{R}$ and $\mathbf{r}$, respectively. The vector potential of a uniform magnetic field $\mathbf{B}$ at position $\mathbf{u}$ is given by $\mathbf{A}(\mathbf{u}) = \frac{1}{2}\mathbf{B} \times (\mathbf{u} - \mathbf{G})$, where $\mathbf{G}$ is the gauge origin.

A. Born–Oppenheimer approximation

We are interested in writing down the effective nuclear Hamiltonian within the Born–Oppenheimer approximation, beginning from the nonrelativistic Hamiltonian of a molecular system in a uniform magnetic field,

$$H_{\text{mol}} = T_{\text{nuc}} + H_{\text{el}} + V_{\text{nuc}}. \tag{1}$$

Here, the nuclear kinetic energy operator is given by

$$T_{\text{nuc}} = \sum_{I=1}^{N_{\text{nuc}}} \frac{\Pi_I^2}{2M_I}, \quad \mathbf{\Pi}_I = \mathbf{P}_I - Z_I e \mathbf{A}(\mathbf{R}_I), \tag{2}$$

where $\mathbf{P}_I = -i\hbar\partial/\partial\mathbf{R}_I$ is the canonical momentum and $\mathbf{\Pi}_I$ is the physical momentum of nucleus I, while the nuclear repulsion operator is given by

$$V_{\text{nuc}} = \sum_{I>J=1}^{N_{\text{nuc}}} \frac{Z_I Z_J e^2}{4\pi\varepsilon_0 |\mathbf{R}_I - \mathbf{R}_J|}, \tag{3}$$

where e is the elementary charge and ε_0 is the vacuum permittivity. The electronic Hamiltonian is given by

$$H_{\text{el}} = \frac{1}{2m_e}\sum_{i=1}^{N_{\text{el}}} (\mathbf{p}_i + e\mathbf{A}(\mathbf{r}_i))^2 + \sum_{i>j=1}^{N_{\text{el}}} \frac{e^2}{4\pi\varepsilon_0|\mathbf{r}_i - \mathbf{r}_j|} - \sum_{i=1}^{N_{\text{el}}}\sum_{I=1}^{N_{\text{nuc}}} \frac{Z_I e^2}{4\pi\varepsilon_0|\mathbf{r}_i - \mathbf{R}_I|}. \tag{4}$$

The molecular wave function satisfies the time-dependent Schrödinger equation

$$H_{\text{mol}}|\Psi\rangle = i\hbar\frac{\partial}{\partial t}|\Psi\rangle. \tag{5}$$

Staying within the Born–Oppenheimer approximation, we write the molecular wave function as a product of a time-dependent nuclear wave function $\psi(\mathbf{R}, t)$ and an electronic wave function $\phi(\mathbf{r}; \mathbf{R})$ that is time independent as follows:

$$\Psi(\mathbf{R}, \mathbf{r}, t) = \psi(\mathbf{R}, t)\phi(\mathbf{r}; \mathbf{R}). \tag{6}$$

The relevant configurations $\mathbf{R}$ where the nuclear wave function is concentrated evolve in time, but the electronic wave function formally does not. We assume that the electronic wave function is obtained at each nuclear configuration $\mathbf{R}$ by solving the time-independent electronic Schrödinger equation in some exact or approximate manner such that

$$U_{\text{BO}}(\mathbf{R}) = \langle\phi|H_{\text{el}}|\phi\rangle, \tag{7}$$

and we wish to solve the molecular Schrödinger equation (5) approximately by inserting the product form of Eq. (6) and projecting the resulting equation from the left by the electronic wave function as follow:

$$\langle\phi|H_{\text{mol}}|\psi\phi\rangle = i\hbar\langle\phi|\frac{\partial}{\partial t}|\psi\phi\rangle. \tag{8}$$

By constructing an effective nuclear Hamiltonian H such that

$$H|\psi\rangle = \langle\phi|T_{\text{nuc}} + H_{\text{el}}|\psi\phi\rangle, \tag{9}$$

we may determine the Born–Oppenheimer nuclear wave function from the effective nuclear Schrödinger equation

$$H|\psi\rangle = i\hbar\frac{\partial}{\partial t}|\psi\rangle. \tag{10}$$

Within the Born–Oppenheimer approximation, all time dependence of the molecular system is determined using the nuclear Schrödinger equation (10). Loosely speaking, the electronic state adjusts instantaneously to the motion of the nuclei.

B. Geometric vector and scalar potentials

To determine the Born–Oppenheimer nuclear Hamiltonian H from Eq. (9), we consider first the projection of the squared kinetic momentum of nucleus I on the electronic wave function. Projecting against the electronic state, we obtain

$$\begin{aligned}\langle\phi|\Pi_I^2|\psi\phi\rangle &= \langle\phi|[\mathbf{P}_I - Z_I\mathbf{A}(\mathbf{R}_I)]^2|\psi\phi\rangle \\ &= \langle\phi|\phi P_I^2\psi\rangle + 2\langle\phi|\mathbf{P}_I\psi\mathbf{P}_I\phi\rangle + \langle\phi|\psi P_I^2\phi\rangle \\ &\quad - \langle\phi|Z_I\mathbf{P}_I\cdot\mathbf{A}(\mathbf{R}_I)|\psi\phi\rangle - 2\langle\phi|Z_I\mathbf{A}(\mathbf{R}_I)|\phi\mathbf{P}_I\psi\rangle \\ &\quad - 2\langle\phi|Z_I\mathbf{A}(\mathbf{R}_I)|\psi\mathbf{P}_I\phi\rangle + \langle\phi|Z_I^2\mathbf{A}(\mathbf{R}_I)^2|\psi\phi\rangle \\ &= \{[\mathbf{P}_I - Z_I\mathbf{A}(\mathbf{R}_I)]^2 + 2\langle\phi|\mathbf{P}_I\phi\rangle\cdot[\mathbf{P}_I - Z_I\mathbf{A}(\mathbf{R}_I)] \\ &\quad + \langle\phi|\mathbf{P}_I^2\phi\rangle\}|\psi\rangle, \end{aligned} \tag{11}$$

which can be written as

$$\langle\phi|\Pi_I^2|\psi\phi\rangle = \left(\Pi_I^2 + 2\boldsymbol{\chi}_I\cdot\boldsymbol{\Pi}_I + \Lambda\right)|\psi\rangle, \tag{12}$$

where we have introduced the geometric vector and scalar potentials, respectively, as follows:

$$\boldsymbol{\chi}_I = \langle\phi|\mathbf{P}_I|\phi\rangle, \tag{13}$$

$$\Lambda_I = \langle\phi|P_I^2|\phi\rangle. \tag{14}$$

The geometric vector potential is also known as the Berry potential or Berry connection. The application of the momentum operator $\mathbf{P}_I = -i\hbar\nabla_I$ to $\langle\phi|\phi\rangle \equiv 1$ gives

$$\mathbf{P}_I\langle\phi|\phi\rangle = -\langle\mathbf{P}_I\phi|\phi\rangle + \langle\phi|\mathbf{P}_I\phi\rangle = \mathbf{0}. \tag{15}$$

Hence, it follows that the geometric vector potential is real-valued,

$$\boldsymbol{\chi}_I = \langle\phi|\mathbf{P}_I\phi\rangle = \langle\mathbf{P}_I\phi|\phi\rangle = \langle\phi|\mathbf{P}_I\phi\rangle^* = \boldsymbol{\chi}_I^*. \tag{16}$$

Next, we observe that

$$\mathbf{P}_I\cdot\boldsymbol{\chi}_I = -\langle\mathbf{P}_I\phi|\mathbf{P}_I\phi\rangle + \langle\phi|P_I^2\phi\rangle. \tag{17}$$

Introducing

$$\Delta_I = \langle\mathbf{P}_I\phi|\mathbf{P}_I\phi\rangle = \Delta_I^*, \tag{18}$$

we find that the scalar potential may be decomposed into real and imaginary parts as

$$\Lambda_I = \Delta_I + \mathbf{P}_I\cdot\boldsymbol{\chi}_I. \tag{19}$$

To express Eq. (12) in a more convenient form, we introduce an effective nuclear physical momentum

$$\begin{aligned}\overline{\boldsymbol{\Pi}}_I &= \boldsymbol{\Pi}_I + \boldsymbol{\chi}_I \\ &= \mathbf{P}_I - Z_I e\mathbf{A}(\mathbf{R}_I) + \boldsymbol{\chi}_I \end{aligned} \tag{20}$$

and also the geometric scalar potential

$$\overline{\Delta}_I = \Delta_I - \chi_I^2 \tag{21}$$

and obtain the following projected squared momentum operator

$$\langle\phi|\Pi_I^2|\psi\phi\rangle = \left(\overline{\Pi}_I^2 + \overline{\Delta}_I\right)|\psi\rangle. \tag{22}$$

By introducing the resolution of identity in Eq. (18), we find that the geometric scalar potential is non-negative and may be written as

$$\overline{\Delta}_I = \sum_{p\neq 0}|\langle\phi_p|\mathbf{P}_I|\phi\rangle|^2 \geq 0, \tag{23}$$

where the summation is over all excited states. This quantity appears in the diagonal Born–Oppenheimer correction (DBOC) as follows:

$$U_{\mathrm{DBOC}} = \sum_I \frac{\hbar^2}{2M_I}\overline{\Delta}_I. \tag{24}$$

C. Born–Oppenheimer nuclear Schrödinger equation

Returning to the Schrödinger equation in Eq. (10), we find that it may be written in the form

$$H|\psi\rangle = (T+U)|\psi\rangle = i\hbar\frac{\partial}{\partial t}|\psi\rangle \tag{25}$$

in terms of the kinetic- and potential-energy operators

$$T = \sum_{I=1}^{N_{\mathrm{nuc}}}\frac{1}{2M_I}\overline{\Pi}_I^2, \tag{26}$$

$$U = U_{\mathrm{BO}} + \sum_{I=1}^{N_{\mathrm{nuc}}}\frac{1}{2M_I}\overline{\Delta}_I + V_{\mathrm{nuc}}. \tag{27}$$

We note that all quantities entering the Hamiltonian depend on the nuclear coordinates $\mathbf{R}$, including the momentum operators.

The mass-dependent DBOC contribution to the potential is normally neglected, but in a few cases, it has been calculated as a nonadiabatic correction to the potential-energy surface.[31–33] In these cases, the wave function has been real so that the geometric vector potential vanishes and $\overline{\Delta}_I = \Delta_I$. The correction is expected to be small and have a negligible impact on molecular dynamics in regions where the Born–Oppenheimer approximation is valid. However, it is, in general, more important to include than in the field-free case, especially for strong fields and/or dynamics far from equilibrium.[13] We finally note that the Born–Oppenheimer approximation is usually taken to mean that all matrix elements that couple different electronic states are neglected; since the DBOC arises from such couplings [Eq. (23)], its inclusion is normally thought of as going beyond the Born–Oppenheimer approximation.

D. Geometric gauge transformations

The effective nuclear Hamiltonian $H = T + U$ given in Eqs. (25)–(27) depends on several expectation values over the geometry-dependent electronic wave function—namely, the Born–Oppenheimer potential $U_{\mathrm{BO}}(\mathbf{R})$, the geometric vector potential $\boldsymbol{\chi}_I(\mathbf{R})$, and the geometric scalar potential $\overline{\Delta}_I(\mathbf{R})$, whose geometry dependence arises from the parametric dependence of the electronic wave function on the nuclear coordinates. Since the electronic wave function at each geometry is determined by solving the electronic Schrödinger equation, it is (in the absence of degeneracies) uniquely determined up to a geometry-dependent phase factor. It is therefore important to establish the invariance of the nuclear Schrödinger equation to a geometry-dependent gauge transformation of the electronic wave function.

Consider the following geometry-dependent gauge transformation of the electronic wave function:

$$|\phi'\rangle = \mathrm{e}^{-\mathrm{i}F(\mathbf{R})/\hbar}|\phi\rangle, \tag{28}$$

where the gauge function F is a real-valued differentiable function of the nuclear coordinates $\mathbf{R}$. The corresponding gauge-transformed matrix elements entering the nuclear Hamiltonian $H = T + U$ are

$$U'_{\mathrm{BO}}(\mathbf{R}) = U_{\mathrm{BO}}(\mathbf{R}), \tag{29}$$

$$\boldsymbol{\chi}'_I(\mathbf{R}) = \boldsymbol{\chi}_I(\mathbf{R}) - \nabla_I F(\mathbf{R}), \tag{30}$$

$$\overline{\Delta}'_I(\mathbf{R}) = \overline{\Delta}_I(\mathbf{R}). \tag{31}$$

The invariance of $U_{\mathrm{BO}}(\mathbf{R})$ follows since H_{el} in Eq. (7) does not differentiate with respect to the nuclear coordinates. To determine the gauge transformations of $\boldsymbol{\chi}_I(\mathbf{R})$ in Eq. (13) and of $\overline{\Delta}_I(\mathbf{R})$ in Eq. (23), we note that

$$\mathbf{P}_I|\phi'\rangle = e^{-\mathrm{i}F(\mathbf{R})/\hbar}(\mathbf{P}_I|\phi\rangle - |\phi\rangle\nabla_I F(\mathbf{R})), \tag{32}$$

which, upon projection by $\langle\phi'|$ and $\langle\phi'_p|$, respectively, followed by the use of orthonormality $\langle\phi|\phi\rangle = 1$ and $\langle\phi_p|\phi\rangle = 0$, gives Eqs. (30) and (31).

Using these results, we find that the nuclear momentum operator transforms as

$$\begin{aligned}\overline{\Pi}'_I &= \overline{\Pi}_I - \nabla_I F(\mathbf{R}) \\ &= \mathrm{e}^{\mathrm{i}F(\mathbf{R})/\hbar}\,\overline{\Pi}_I\,\mathrm{e}^{-\mathrm{i}F(\mathbf{R})/\hbar}\end{aligned} \tag{33}$$

and hence that the operator of the time-dependent Born–Oppenheimer Schrödinger equation transforms as

$$H' - \mathrm{i}\hbar\frac{\partial}{\partial t} = \mathrm{e}^{\mathrm{i}F(\mathbf{R})/\hbar}\left(H - \mathrm{i}\hbar\frac{\partial}{\partial t}\right)\mathrm{e}^{-\mathrm{i}F(\mathbf{R})/\hbar}, \tag{34}$$

whether or not the DBOC is included in the Hamiltonian. This gauge transformation may be compensated for by a unitary transformation of the nuclear wave function

$$|\psi'\rangle = \mathrm{e}^{\mathrm{i}F(\mathbf{R})/\hbar}|\psi\rangle \tag{35}$$

and hence does not affect any observable quantities if the variational space is sufficiently flexible to accommodate such transformations.

In passing, we note that, while a geometry-dependent gauge transformation can change the local behavior of the Berry connection $\boldsymbol{\chi}_I(\mathbf{R})$, there is an invariant phase along any closed loop C,

$$\zeta = \oint_C \boldsymbol{\chi}(\mathbf{R})\cdot\mathrm{d}\mathbf{R} = \sum_I \oint_C \boldsymbol{\chi}_I(\mathbf{R})\cdot\mathrm{d}\mathbf{R}_I, \tag{36}$$

known as the Berry phase.[1] Among the many contexts where this quantity arises is the calculation of magnetic properties, such as rotational g factors.[34]

E. Magnetic gauge transformations

Consider now a gauge transformation of the external magnetic vector potential

$$\tilde{\mathbf{A}}(\mathbf{u}) = \mathbf{A}(\mathbf{u}) + \nabla f(\mathbf{u}) \tag{37}$$

and the corresponding gauge-transformed nuclear and electronic wave functions

$$|\tilde{\phi}\rangle = \left(\prod_{i=1}^{N_{\mathrm{el}}}\mathrm{e}^{-\mathrm{i}ef(\mathbf{r}_i)/\hbar}\right)|\phi\rangle, \tag{38}$$

$$|\tilde{\psi}\rangle = \left(\prod_{I=1}^{N_{\mathrm{nuc}}}\mathrm{e}^{\mathrm{i}Z_I ef(\mathbf{R}_I)/\hbar}\right)|\psi\rangle. \tag{39}$$

In this case, all electronic expectation values entering the nuclear Hamiltonian, including the geometric vector potential, are unaffected,

$$\tilde{U}_{\mathrm{BO}}(\mathbf{R}) = U_{\mathrm{BO}}(\mathbf{R}), \tag{40}$$

$$\tilde{\boldsymbol{\chi}}_I(\mathbf{R}) = \boldsymbol{\chi}_I(\mathbf{R}), \tag{41}$$

$$\tilde{\overline{\Delta}}_I(\mathbf{R}) = \overline{\Delta}_I(\mathbf{R}), \tag{42}$$

while the nuclear momenta transform as

$$\begin{aligned}\tilde{\overline{\Pi}}_I &= \overline{\Pi}_I - Z_I e\nabla_I f(\mathbf{R}_I) \\ &= \mathrm{e}^{\mathrm{i}Z_I ef(\mathbf{R}_I)/\hbar}\,\overline{\Pi}_I\,\mathrm{e}^{-\mathrm{i}Z_I ef(\mathbf{R}_I)/\hbar}\end{aligned} \tag{43}$$

and the Hamiltonian becomes

$$\begin{aligned}\tilde{H} - \mathrm{i}\hbar\frac{\partial}{\partial t} = &\left(\prod_{I=1}^{N_{\mathrm{nuc}}}\mathrm{e}^{\mathrm{i}Z_I ef(\mathbf{R}_I)/\hbar}\right)\left(H - \mathrm{i}\hbar\frac{\partial}{\partial t}\right) \\ &\times\left(\prod_{I=1}^{N_{\mathrm{nuc}}}\mathrm{e}^{-\mathrm{i}Z_I ef(\mathbf{R}_I)/\hbar}\right).\end{aligned} \tag{44}$$

Again, the gauge transformation is compensated for by the unitary transformation of the nuclear wave function in Eq. (39) and does not affect any observable quantities as long as our computational model can perform such transformations.

F. Equations of motion

We derive the equations of motion by considering the time evolution of the expectation values of the position and momentum operators using Eq. (10) and noting that

$$\frac{\mathrm{d}}{\mathrm{d}t}\langle\psi|R_{J\beta}|\psi\rangle = \frac{\mathrm{i}}{\hbar}\langle\psi|[H, R_{J\beta}]|\psi\rangle, \tag{45}$$

$$\frac{\mathrm{d}}{\mathrm{d}t}\langle\psi|\overline{\Pi}_{J\beta}|\psi\rangle = \frac{\mathrm{i}}{\hbar}\langle\psi|[H, \overline{\Pi}_{J\beta}]|\psi\rangle. \tag{46}$$

To determine the commutators of $R_{J\beta}$ and $\overline{\Pi}_{J\beta}$ with the Hamiltonian, it is useful first to evaluate their commutators with the momentum operators as follows:

$$[\overline{\Pi}_{I\alpha}, R_{J\beta}] = -\mathrm{i}\hbar\delta_{IJ}\delta_{\alpha\beta}, \tag{47}$$

$$[\overline{\Pi}_{I\alpha}, \overline{\Pi}_{J\beta}] = \mathrm{i}\hbar eZ_J\delta_{IJ}\epsilon_{\alpha\beta\gamma}B_\gamma + \mathrm{i}\hbar\Omega_{I\alpha J\beta}, \tag{48}$$

where $\epsilon_{\alpha\beta\gamma}$ is the Levi-Cività tensor, and summation over the repeated index γ is implied. We have also introduced the Berry curvature $\boldsymbol{\Omega}$ with elements

$$\Omega_{I\alpha J\beta} = \nabla_{J\beta}\chi_{I\alpha} - \nabla_{I\alpha}\chi_{J\beta} = \mathrm{i}\hbar\big[\langle\nabla_{I\alpha}\phi|\nabla_{J\beta}\phi\rangle - \langle\nabla_{J\beta}\phi|\nabla_{I\alpha}\phi\rangle\big]. \tag{49}$$

In evaluating the commutator in Eq. (48), it is useful to express the magnetic vector potential as $A_\alpha(\mathbf{R}_I) = \frac{1}{2}\epsilon_{\alpha\beta\gamma}B_\beta R_{I\gamma}$ and the geometric vector potential in the symmetric form

$$\chi_{I\alpha} = \frac{\mathrm{i}\hbar}{2}\big[\langle\nabla_{I\alpha}\phi|\phi\rangle - \langle\phi|\nabla_{I\alpha}\phi\rangle\big], \tag{50}$$

which is valid since the geometric vector potential is real valued. We note from Eq. (49) that the Berry curvature is an antisymmetric $3N_{\mathrm{nuc}} \times 3N_{\mathrm{nuc}}$ matrix,

$$\mathbf{\Omega}^{\mathrm{T}} = -\mathbf{\Omega}. \tag{51}$$

For each pair of atoms I and J, $\mathbf{\Omega}_{IJ}$ is the 3×3 matrix whose elements are given by $[\mathbf{\Omega}_{IJ}]_{\alpha\beta} = \Omega_{I\alpha J\beta}$, and we note the symmetry

$$\mathbf{\Omega}_{IJ}^{\mathrm{T}} = -\mathbf{\Omega}_{JI}. \tag{52}$$

Evaluating the gauge-transformed Berry curvature, we obtain

$$\begin{aligned}\Omega'_{I\alpha J\beta} &= \nabla_{J\beta}\chi'_{I\alpha} - \nabla_{I\alpha}\chi'_{J\beta}\\ &= \nabla_{J\beta}(\chi_{I\alpha} - \nabla_{I\alpha}F) - \nabla_{I\alpha}(\chi_{J\beta} - \nabla_{J\beta}F)\\ &= \nabla_{J\beta}\chi_{I\alpha} - \nabla_{I\alpha}\chi_{J\beta} = \Omega_{I\alpha J\beta},\end{aligned} \tag{53}$$

demonstrating its gauge invariance.

Returning to Eqs. (45) and (46) and making use of the identity $[a^2, b] = \{a, [a, b]\} = a[a, b] + [a, b]a$ where curly brackets denote the anti-commutator, we obtain the time derivatives

$$\frac{\mathrm{d}}{\mathrm{d}t}\langle\psi|R_{J\beta}|\psi\rangle = \frac{1}{M_J}\langle\psi|\overline{\Pi}_{J\beta}|\psi\rangle, \tag{54}$$

$$\begin{aligned}\frac{\mathrm{d}}{\mathrm{d}t}\langle\psi|\overline{\Pi}_{J\beta}|\psi\rangle = &-\frac{\partial}{\partial R_{J\beta}}\langle\psi|U_{\mathrm{BO}}|\psi\rangle - \frac{Z_J}{M_J}\epsilon_{\alpha\beta\gamma}\langle\psi|\overline{\Pi}_{J\alpha}|\psi\rangle B_\gamma\\ &- \sum_I \frac{1}{2M_I}\langle\psi|\{\overline{\Pi}_{I\alpha}, \Omega_{I\alpha J\beta}\}|\psi\rangle.\end{aligned} \tag{55}$$

Finally, we assume that the nuclear wave function is sharply peaked around $\overline{\mathbf{R}} = \langle\psi|\mathbf{R}|\psi\rangle$ so that

$$\langle\psi|U_{\mathrm{BO}}|\psi\rangle \approx U_{\mathrm{BO}}(\overline{\mathbf{R}}), \tag{56}$$

$$\langle\psi|\Omega_{I\alpha J\beta}|\psi\rangle \approx \Omega_{I\alpha,J\beta}(\overline{\mathbf{R}}), \tag{57}$$

$$\langle\psi|\{\overline{\Pi}_{I\alpha}, \Omega_{I\alpha J\beta}\}|\psi\rangle \approx 2\,\Omega_{I\alpha,J\beta}(\overline{\mathbf{R}})\,\langle\psi|\overline{\Pi}_{I\alpha}|\psi\rangle. \tag{58}$$

Alternatively, the last approximation can also be obtained from a more restrictive combination of locality assumptions and a resolution of the identity, neglecting all couplings to excited states.

Using the locality assumptions in Eqs. (56)–(58), the equations of motion become

$$M_I\ddot{\overline{\mathbf{R}}}_I = \mathbf{F}_I^{\mathrm{BO}}(\overline{\mathbf{R}}) + \mathbf{F}_I^{\mathrm{L}}(\dot{\overline{\mathbf{R}}}) + \mathbf{F}_I^{\mathrm{B}}(\dot{\overline{\mathbf{R}}}, \overline{\mathbf{R}}), \tag{59}$$

where we have introduced the Born–Oppenheimer force

$$\mathbf{F}_I^{\mathrm{BO}}(\overline{\mathbf{R}}) = -\nabla_I U_{\mathrm{BO}}(\overline{\mathbf{R}}), \tag{60}$$

the (bare) Lorentz force

$$\mathbf{F}_I^{\mathrm{L}}(\dot{\overline{\mathbf{R}}}) = -eZ_I\,\mathbf{B} \times \dot{\overline{\mathbf{R}}}_I, \tag{61}$$

and the Berry (screening) force

$$\mathbf{F}_I^{\mathrm{B}}(\dot{\overline{\mathbf{R}}}, \overline{\mathbf{R}}) = \sum_J \mathbf{\Omega}_{IJ}(\overline{\mathbf{R}})\,\dot{\overline{\mathbf{R}}}_J, \tag{62}$$

where ∇_I in Eq. (60) differentiates with respect to $\overline{\mathbf{R}}_I$. The screened Lorentz force on nucleus I is the sum of the bare Lorentz force and the Berry force on this nucleus. Henceforth, we omit the argument $\overline{\mathbf{R}}$ to the forces.

Equation (59) is legitimate under the assumptions stated but will be inadequate in the presence of, for example, singularities, such as conical intersections. There has been recent work seeking to address this issue in the context of dynamics equations where the Berry curvature is present.[35] Methods such as surface hopping[36,37] can also be applicable in this framework. However, these concerns are beyond the scope of the present work.

G. Screened Lorentz force

The screened Lorentz force on nucleus I is calculated from the Berry curvature tensor, with a contribution from each atom in the molecule, as follows:

$$\mathbf{F}_I^{\mathrm{LB}} = -eZ_I\mathbf{B} \times \dot{\overline{\mathbf{R}}}_I + \sum_J \mathbf{\Omega}_{IJ}\dot{\overline{\mathbf{R}}}_J. \tag{63}$$

We recall from Eq. (51) that $\mathbf{\Omega}$ is anti-symmetric, implying that each three-by-three diagonal block $\mathbf{\Omega}_{II}$ is anti-symmetric, while the off-diagonal three-by-three blocks $\mathbf{\Omega}_{IJ}$, with $I \neq J$, are, in general, not anti-symmetric. We note that the product of a three-by-three matrix with a vector may be expressed as a cross product if and only if the matrix is anti-symmetric,

$$\begin{pmatrix} 0 & -a_3 & a_2 \\ a_3 & 0 & -a_1 \\ -a_2 & a_1 & 0 \end{pmatrix}\begin{pmatrix} b_1 \\ b_2 \\ b_3 \end{pmatrix} = \begin{pmatrix} a_1 \\ a_2 \\ a_3 \end{pmatrix} \times \begin{pmatrix} b_1 \\ b_2 \\ b_3 \end{pmatrix} = \mathbf{a} \times \mathbf{b}. \tag{64}$$

Therefore, decomposing the blocks of the Berry curvature tensor into symmetric and anti-symmetric parts,

$$\mathbf{\Omega}_{IJ}^{\mathrm{S}} = \frac{1}{2}\big(\mathbf{\Omega}_{IJ} + \mathbf{\Omega}_{IJ}^{\mathrm{T}}\big),\ \mathbf{\Omega}_{IJ}^{\mathrm{A}} = \frac{1}{2}\big(\mathbf{\Omega}_{IJ} - \mathbf{\Omega}_{IJ}^{\mathrm{T}}\big), \tag{65}$$

and introducing a vector consisting of the independent elements of the anti-symmetric part of the Berry curvature tensor,

$$\boldsymbol{\omega}_{IJ}^{\mathrm{A}} = \begin{pmatrix} \Omega_{Iz,Jy}^{\mathrm{A}} \\ \Omega_{Ix,Jz}^{\mathrm{A}} \\ \Omega_{Iy,Jx}^{\mathrm{A}} \end{pmatrix}, \tag{66}$$

we may write the screened Lorentz force as

$$\mathbf{F}_I^{\mathrm{LB}} = -eZ_I\mathbf{B} \times \dot{\overline{\mathbf{R}}}_I + \sum_J \boldsymbol{\omega}_{IJ}^{\mathrm{A}} \times \dot{\overline{\mathbf{R}}}_J + \sum_{J\neq I} \mathbf{\Omega}_{IJ}^{\mathrm{S}}\dot{\overline{\mathbf{R}}}_J, \tag{67}$$

where $\mathbf{\Omega}_{JJ}^{\mathrm{S}} = \mathbf{0}$.

Taking the field vector **B** to define the z-axis and introducing the effective charges Q_{IJ} by the condition

$$e\,Q_{IJ}\mathbf{B} = -\boldsymbol{\omega}_{IJ}^{\mathrm{A}}, \tag{68}$$

we obtain

$$\mathbf{F}_I^{\mathrm{LB}} = -\sum_J e(\delta_{IJ}Z_I + Q_{IJ})\mathbf{B}\times\dot{\mathbf{R}}_J + \sum_{J\neq I}\boldsymbol{\Omega}_{IJ}^{\mathrm{S}}\dot{\mathbf{R}}_J \tag{69}$$

for the screened Lorentz force on nucleus I. For an atom, we have (in the limit of a complete one-electron basis) $Q_{11} = -N_{\mathrm{el}}$, giving

$$\mathbf{F}_1^{\mathrm{LB}} = e(Z_1 - N_{\mathrm{el}})\dot{\mathbf{R}}_1\times\mathbf{B} \quad (\text{atom}), \tag{70}$$

where $Z_1 - N_{\mathrm{el}}$ is the total charge of the atom. As we shall see in Sec. II H, $Q_{11} = -N_{\mathrm{el}}$ is satisfied even for an incomplete basis of London atomic orbitals.

H. Berry curvature of a London atomic orbital

Let $\varphi_{lm}(\mathbf{r};\mathbf{R})$ be a normalized real-valued field-free atomic orbital at position **R** of solid-harmonic quantum numbers ℓ and m, and let

$$\psi_{\ell m}(\mathbf{r};\mathbf{R}) = \mathrm{e}^{-\mathrm{i}e\mathbf{A}(\mathbf{R}_1)\cdot\mathbf{r}/\hbar}\varphi_{\ell m}(\mathbf{r};\mathbf{R}) \tag{71}$$

be the corresponding field-dependent London atomic orbital, where $\mathbf{A}(\mathbf{R}) = \frac{1}{2}\mathbf{B}\times\mathbf{R}$ is the magnetic vector potential at the position of the orbital **R**. The geometric vector potential generated by the London orbital is

$$\boldsymbol{\chi}_{\ell m}(\mathbf{R}) = \int\psi_{\ell m}^{*}\mathbf{P}\psi_{\ell m}\,\mathrm{d}\mathbf{r} = e\mathbf{A}(\mathbf{R}), \tag{72}$$

where $\mathbf{P} = -i\hbar\nabla_{\mathbf{R}}$. To see how this result arises, we first note that (by rearranging the scalar triple product)

$$\nabla_{\mathbf{R}}(-\mathbf{A}(\mathbf{R})\cdot\mathbf{r}) = \nabla_{\mathbf{R}}(\mathbf{A}(\mathbf{r})\cdot\mathbf{R}) = \mathbf{A}(\mathbf{r}). \tag{73}$$

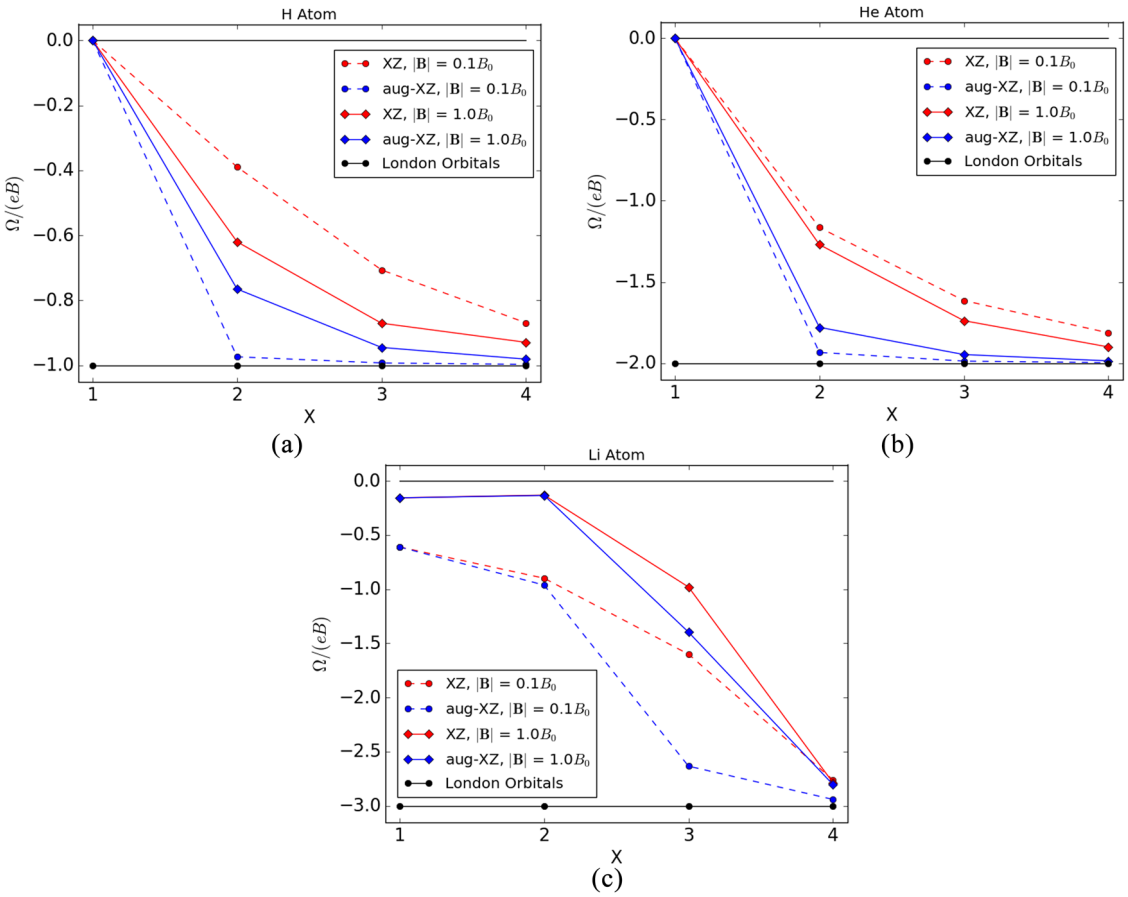

FIG. 1. Electronic charges calculated from the Berry curvature as a function of basis set without London orbitals for the hydrogen (a), helium (b), and lithium (c) atoms. Lithium values were calculated using UHF with a spin-projection corresponding to a doublet. Data are plotted as a function of basis set cardinal number X for the cc-pVXZ and aug-cc-pVXZ basis sets, as well as the STO-3G basis set ($X = 1$). The magnetic field was oriented along the z-axis, with strengths of $|\mathbf{B}| = 0.1B_0$ and $|\mathbf{B}| = 1.0B_0$ as reflected in the plots. London orbitals reproduce the exact electronic charge for all basis sets/magnetic field strengths.

The integrand of Eq. (72) may therefore be written as

$$\begin{aligned}\psi^*_{\ell m}\mathbf{P}\psi_{\ell m} &= e\mathbf{A}(\mathbf{r})\varphi^*_{\ell m}\varphi_{\ell m} + \varphi^*_{\ell m}\mathbf{P}\varphi_{\ell m}\\ &= e\mathbf{A}(\mathbf{R})\varphi^2_{\ell m} + e\mathbf{A}(\mathbf{r}_\mathbf{R})\varphi^2_{\ell m} + \frac{1}{2}\mathbf{P}\varphi^2_{\ell m},\end{aligned} \tag{74}$$

where, in the last step, we have introduced $\mathbf{r}_\mathbf{R} = \mathbf{r} - \mathbf{R}$ and used the fact that $\varphi_{\ell m}$ is real valued. Integrating over all space, the first term gives $e\mathbf{A}(\mathbf{R})$ by normalization of the orbital, the second term vanishes by parity symmetry, while the last term vanishes by the normalization of the atomic orbital (having interchanged differentiation and integration), yielding Eq. (72).

From the definition of the Berry curvature tensor given in Eq. (49), we obtain

$$\mathbf{\Omega}_{\ell m} = e\begin{pmatrix} 0 & -B_z & B_y \\ B_z & 0 & -B_x \\ -B_y & B_x & 0 \end{pmatrix} \tag{75}$$

and $\boldsymbol{\omega}^{\mathrm{A}}_{\ell m} = e\mathbf{B}$. Assuming a one-electron system described by this London orbital, the effective charge is then $-e$. For the antisymmetric product of N_{el} London spin orbitals, the effective charge is $-N_{\mathrm{el}}e$.

I. Berry curvature from finite differences

The elements of the Berry curvature are combinations of the overlap of wave-function derivatives [see Eq. (49)]. Our task is to calculate these derivative overlaps from finite differences as follows:

$$\langle \nabla_{I\alpha}\phi | \nabla_{J\beta}\phi \rangle \approx \frac{S^{++}_{I\alpha J\beta} - S^{+-}_{I\alpha J\beta} - S^{-+}_{I\alpha J\beta} + S^{--}_{I\alpha J\beta}}{4\delta_{I\alpha}\delta_{J\beta}}. \tag{76}$$

We have here introduced the notation

$$S^{\pm\pm}_{I\alpha J\beta} = \langle \phi_{\pm I\alpha} | \phi_{\pm J\beta} \rangle, \tag{77}$$

where

$$|\phi_{\pm I\alpha}\rangle = |\phi(\mathbf{r}; \mathbf{R} \pm \boldsymbol{\delta}_{I\alpha})\rangle \tag{78}$$

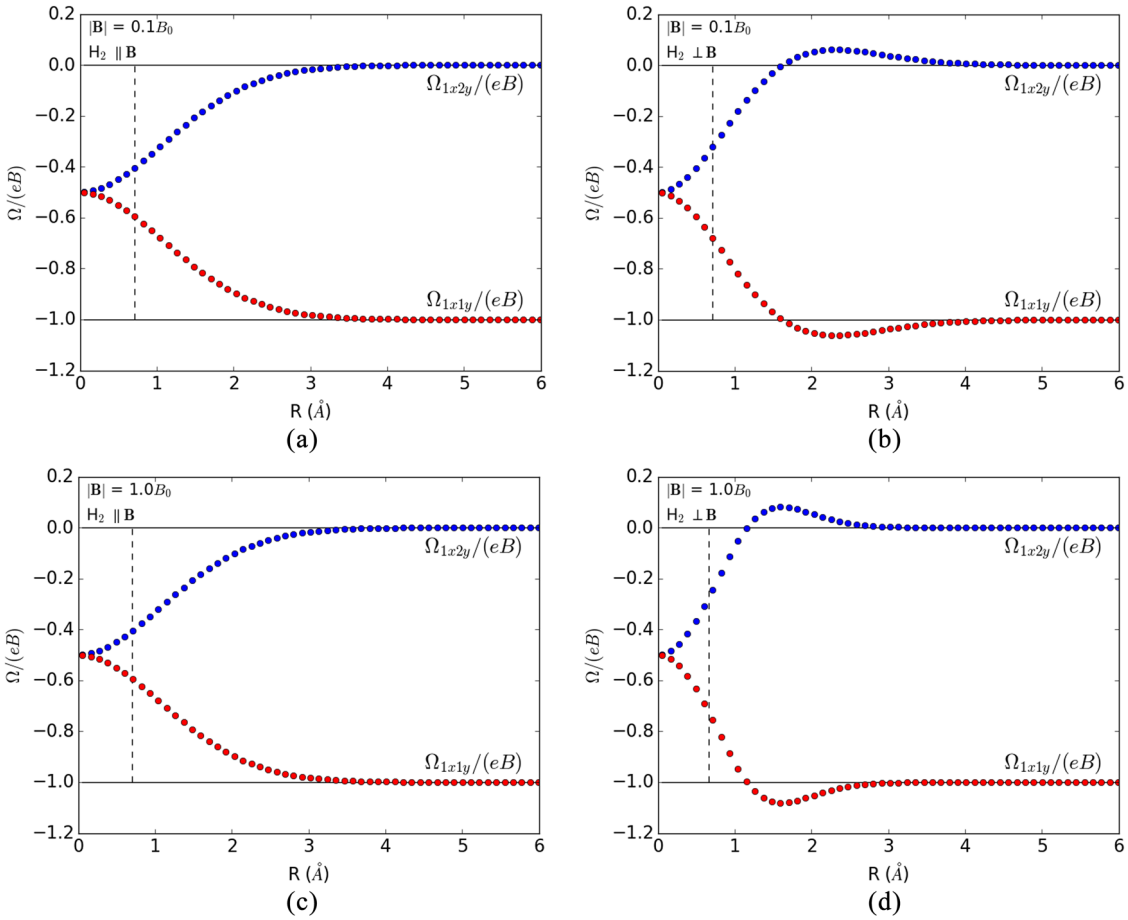

FIG. 2. Berry curvature of H_2 for the RHF singlet state with the STO-3G basis set for orientations parallel [(a) and (c)] and perpendicular [(b) and (d)] to the magnetic field. The field is oriented along the *z*-axis with strengths of $|\mathbf{B}| = 0.1B_0$ [(a) and (b)] and $|\mathbf{B}| = 1.0B_0$ [(c) and (d)]. The molecular orientation perpendicular to the field is along the *x*-axis. Equilibrium bond distances are 0.712 Å (a), 0.711 Å (b), 0.698 Å (c), and 0.662 Å (d) as shown by the vertical dashed lines in each plot.

is the electronic wave function at the geometry $\mathbf{R} \pm \boldsymbol{\delta}_{I\alpha}$, where $\boldsymbol{\delta}_{I\alpha}$ denotes a perturbation of magnitude $\delta_{I\alpha}$ in the $I\alpha$ component of $\mathbf{R}$.

The finite-difference method has been used previously to calculate contributions to the energy from the diagonal Born–Oppenheimer correction for real-valued wave functions.[33,38,39] The present work follows the same finite-difference formulation for the calculation of the Berry curvature but with two important complicating factors. The first is that the Berry curvature tensor contains non-diagonal derivative overlaps with respect to the nuclear coordinates, which leads to the absence of simplifications that would otherwise be present in the diagonal case [e.g., the form of the numerator in Eq. (76)]. The second and more difficult complication is that, in the presence of a magnetic field, the electronic wave function is, in general, complex. For real-valued wave functions, the global phase angle λ is constrained to be $\lambda_n = n\pi$, where n is an integer, which means that any perturbed wave function

$$e^{-i\lambda_n/\hbar}|\phi\rangle \rightarrow e^{-i\lambda_m/\hbar}|\phi_{\pm I\alpha}\rangle \tag{79}$$

may at most undergo a sign change as a result of the change in the phase. In the complex case, the phase angle becomes a continuous variable, and each separate perturbation may result in a drastically different and uncontrolled phase. For example, the derivative of the electronic wave function with respect to a nuclear coordinate can be represented via the finite difference method according to

$$\begin{aligned} |\nabla_{I\alpha}\phi\rangle &\approx \frac{|\tilde{\phi}_{+I\alpha}\rangle - |\tilde{\phi}_{-I\alpha}\rangle}{2\delta_{I\alpha}} \\ &= \frac{|\phi_{+I\alpha}\rangle e^{-i\lambda_+} - |\phi_{-I\alpha}\rangle e^{-i\lambda_-}}{2\delta_{I\alpha}}, \end{aligned} \tag{80}$$

where the tilde denotes a phase-corrected wave function.

We want to evaluate Eq. (80) with the phase-corrected wave function $\tilde{\phi}_{\pm I\alpha}$ since the raw, uncorrected wave function $\phi_{\pm I\alpha}$ gives an ill-defined gradient. For some values of $\lambda_\pm$, the numerator in

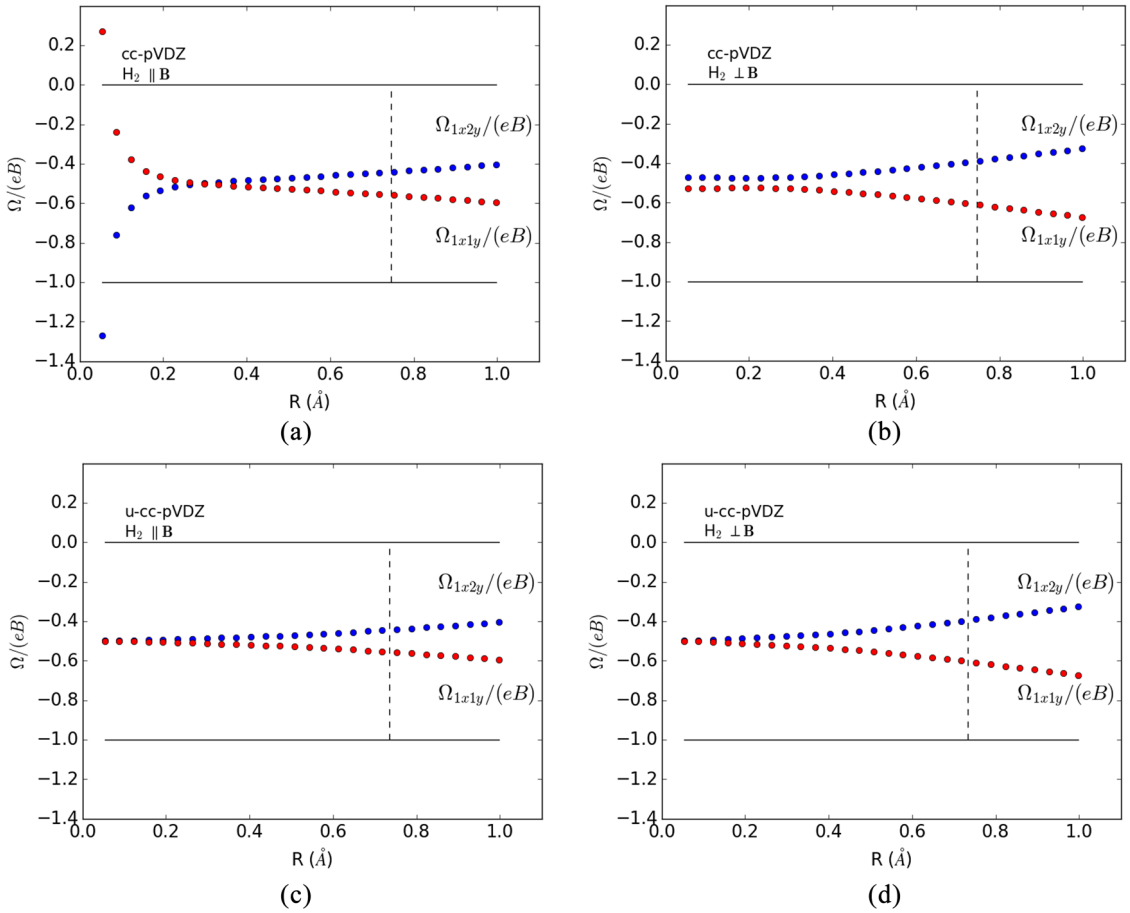

FIG. 3. Berry curvature of H_2 for the RHF singlet state with the cc-pVDZ basis set [(a) and (b)] and the u-cc-pVDZ basis set [(c) and (d)] for orientations parallel [(a) and (c)] and perpendicular [(b) and (d)] to the magnetic field. The field is oriented along the z-axis with a strength of $|\mathbf{B}| = 0.1B_0$ for all panels. The u-cc-pVDZ basis set is the decontracted cc-pVDZ basis. The molecular orientation perpendicular to the field is along the x-axis. Equilibrium bond distances are 0.746 Å (a), 0.745 Å (b), 0.735 Å (c), and 0.734 Å (d) as shown by the vertical dashed lines in each plot.

Eq. (80) is on the order of $\delta_{I\alpha}$, but for most, it is on the order of one. Moreover, since $\phi_{\pm I\alpha}$ has an uncontrolled phase, we cannot simply set $\lambda_{\pm} = 0$. It is therefore necessary to perform the finite difference scheme accounting for the arbitrary phase of each perturbed wave function in a justified, systematic manner.

Toward this end, we note that the overlap of any perturbed wave function with the reference wave function can be represented in polar form by

$$\langle\phi|\phi_{\pm I\alpha}\rangle = \eta_{\pm I\alpha} e^{i\lambda_{\pm I\alpha}}, \tag{81}$$

where $\eta_{\pm I\alpha}$ is the modulus and $\lambda_{\pm I\alpha}$ is the argument. We now multiply $|\phi_{\pm I\alpha}\rangle$ by a phase factor that renders the result of Eq. (81) real. This is accomplished according to

$$|\phi_{\pm I\alpha}\rangle \to e^{-i\lambda_{\pm I\alpha}}|\phi_{\pm I\alpha}\rangle = |\tilde{\phi}_{\pm I\alpha}\rangle, \tag{82}$$

which gives

$$\langle\phi|\tilde{\phi}_{\pm I\alpha}\rangle = \eta_{\pm I\alpha}. \tag{83}$$

The condition on the perturbed wave functions imposed by Eq. (83) is (in the context of finite differences) tantamount to a gauge transform that causes the geometric vector potential to vanish. To see this, we write the finite difference approximation to the geometric vector potential in the form

$$\begin{aligned}\tilde{\chi}_{I\alpha} &\approx \frac{i\hbar\left(\langle\phi|\tilde{\phi}_{-I\alpha}\rangle - \langle\phi|\tilde{\phi}_{+I\alpha}\rangle\right)}{2\delta_{I\alpha}} \\ &= \frac{i\hbar(\eta_{-I\alpha} - \eta_{+I\alpha})}{2\delta_{I\alpha}} = 0\end{aligned} \tag{84}$$

from the fact that $\chi_{I\alpha}$ is real-valued, and since Eq. (84) is pure imaginary, it must be zero. As shown in Sec. II F, the Berry curvature is invariant under geometric gauge transformations and is thus unaffected. We are now in a position to calculate the elements of the Berry curvature tensor using the phase corrections given in Eq. (82)

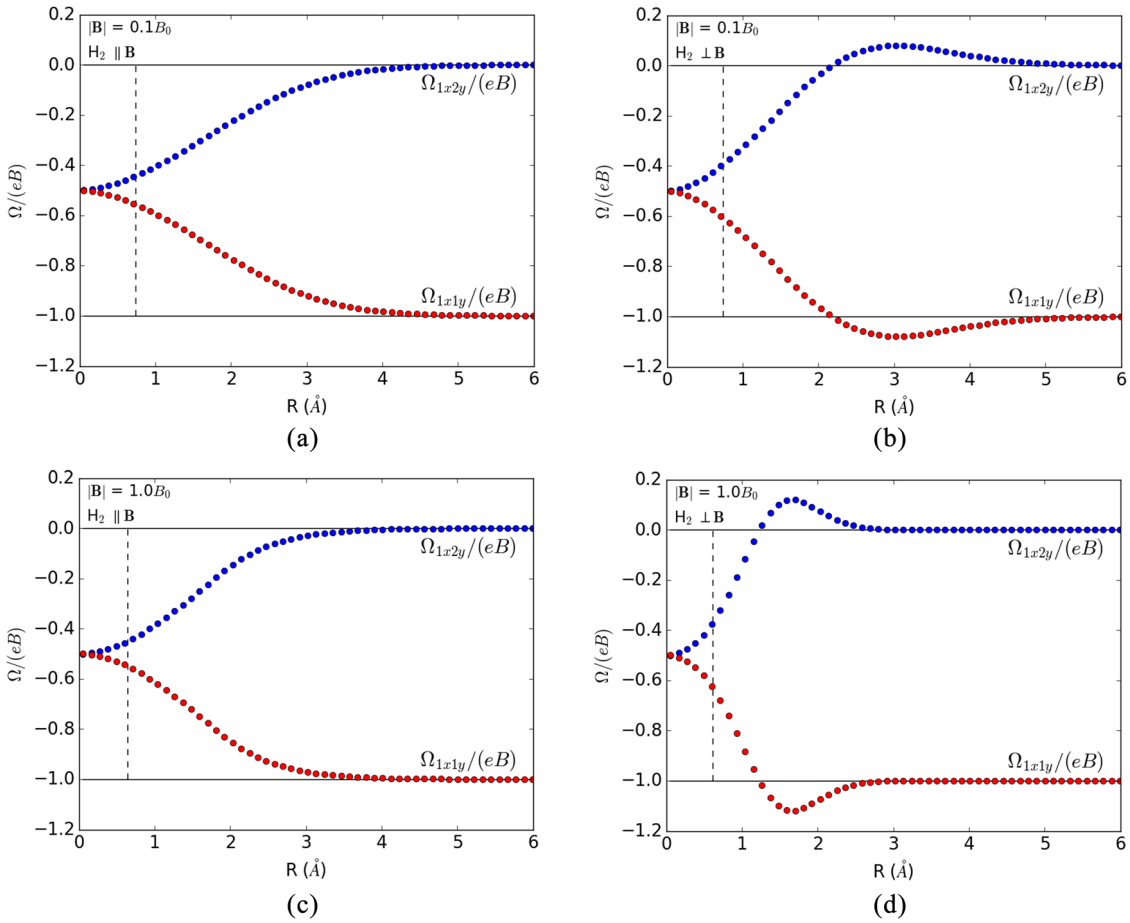

FIG. 4. Berry curvature of H_2 for the RHF singlet state with the u-cc-pVDZ basis set for orientations parallel [(a) and (c)] and perpendicular [(b) and (d)] to the magnetic field. The field is oriented along the *z*-axis with strengths of $|\mathbf{B}| = 0.1B_0$ [(a) and (b)] and $|\mathbf{B}| = 1.0B_0$ [(c) and (d)]. The u-cc-pVDZ basis set is the decontracted cc-pVDZ basis. The molecular orientation perpendicular to the field is along the *x*-axis. Equilibrium bond distances are 0.735 Å (a), 0.734 Å (b), 0.646 Å (c), and 0.609 Å (d) as shown by the vertical dashed lines in each plot.

so that

$$\left\langle \nabla_{I\alpha}\phi \middle| \nabla_{J\beta}\phi \right\rangle \approx \frac{\tilde{S}^{++}_{I\alpha J\beta} - \tilde{S}^{+-}_{I\alpha J\beta} - \tilde{S}^{-+}_{I\alpha J\beta} + \tilde{S}^{--}_{I\alpha J\beta}}{4\delta_{I\alpha}\delta_{J\beta}}, \tag{85}$$

with

$$\begin{aligned} \tilde{S}^{\pm\pm}_{I\alpha J\beta} &= \langle \tilde{\phi}_{\pm I\alpha} | \tilde{\phi}_{\pm J\beta} \rangle \\ &= e^{i\lambda_{\pm I\alpha}} \langle \phi_{\pm I\alpha} | \phi_{\pm J\beta} \rangle e^{-i\lambda_{\pm J\beta}}, \end{aligned} \tag{86}$$

where the phase factors are given in Eq. (81).

III. RESULTS

In this section, we present calculations of the Berry curvature for the hydrogen, helium, and lithium atoms, as well as the H_2 and CH^+ molecules, using the finite-difference scheme outlined in Sec. II. All calculations in this work were performed with the software package LONDON.[15] London orbitals were used in all calculations in Secs. III B and III C, ensuring gauge-origin invariance. Calculations in Sec. III A were performed without using London orbitals.

A. H, He, and Li atoms

In order to demonstrate the importance of London orbitals, the Berry curvature was calculated for the hydrogen, helium, and lithium atoms as a function of basis set size without London orbitals for field strengths of $|\mathbf{B}| = 0.1B_0$ and $|\mathbf{B}| = 1.0B_0$, where $B_0 = 2.35 \times 10^5$ T is one atomic unit magnetic field strength. Calculations were performed with Dunning's correlation-consistent polarized valence basis sets cc-pVXZ[40] (without diffuse functions) and aug-cc-pVXZ[41] (with diffuse functions), in both cases with cardinal numbers $2 \le X \le 4$. In addition, we performed calculations in the minimal STO-3G basis,[42] with the cardinal number $X = 1$.

For neutral atoms, such as those considered here, we recall from Eq. (70) that the exact screened Lorentz force is zero because of the complete cancellation of nuclear and electronic charges in neutral systems. Importantly, *this cancellation is achieved exactly when calculating the Berry curvature with London orbitals in an orbital basis of any size*. By contrast, in a finite basis without London phase factors, only partial cancellation is achieved—see Fig. 1, where we plot the electronic charges of H, He, and Li calculated from the Berry curvature.

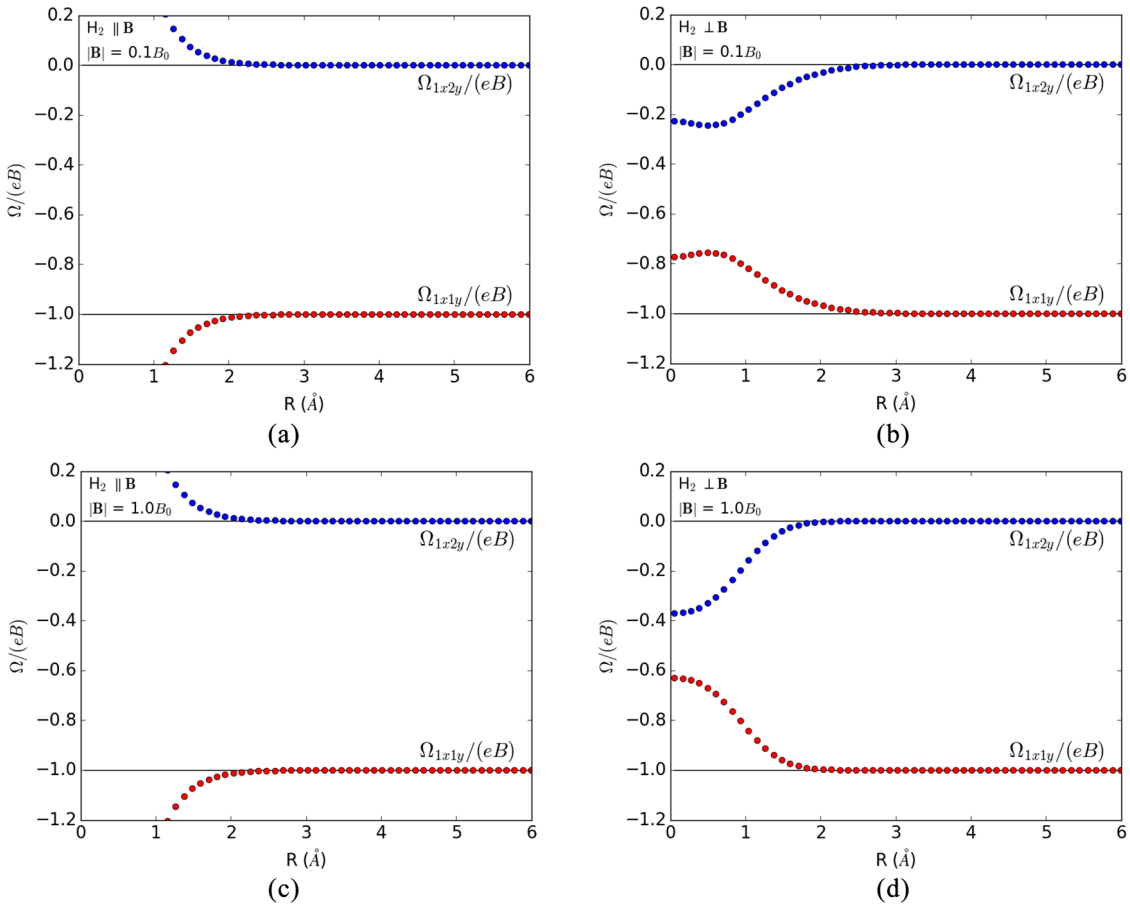

FIG. 5. Berry curvature of H_2 for the UHF $\beta\beta$ triplet state calculated with the STO-3G basis set for orientations parallel [(a) and (c)] and perpendicular [(b) and (d)] to the magnetic field. The field is oriented along the z-axis with strengths of $|\mathbf{B}| = 0.1B_0$ [(a) and (b)] and $|\mathbf{B}| = 1.0B_0$ [(c) and (d)]. The molecular orientation perpendicular to the field is along the x-axis.

As seen in these plots, the convergence of electronic charge calculated from the Berry curvature without using London orbitals is slow and irregular, although slightly faster when diffuse functions are added to the basis sets. In fact, a quantitative agreement with the number of electrons in the atom is only achieved with the aug-cc-pVQZ basis set and then only for H and He. Because of the presence of core electrons (for which the basis sets used here have only single-zeta quality), the basis-set convergence for Li is slower than that for H and He. In general, we expect the basis-set convergence of the Berry curvature in atomic calculations without London orbitals to become more difficult with an increasing number of electrons. In molecules, where, in addition, the atoms may be far away from the gauge origin, convergence will be slower still.

For the calculation of Berry curvature, it is clearly essential to use London orbitals, which give the correct number of electrons even in the smallest basis sets. In all molecular calculations presented here, we therefore use London orbitals.

B. H_2 molecule

The Berry curvature of the lowest singlet and $\beta\beta$ triplet states of H_2 has been calculated at the Hartree–Fock level of theory at orientations of the molecule both parallel and perpendicular to the magnetic field. Calculations were performed with the STO-3G, cc-pVDZ, and cc-pVTZ basis sets of London atomic orbitals for magnetic field strengths of $0.1B_0$ and $1.0B_0$.

It should be noted that a linear dependence in the basis set hampers investigations for small bond distances. For this reason, the Berry curvature was calculated down to a bond distance limit of 0.1 bohr, beyond which the linear dependence starts to manifest itself in the cc-pVTZ basis. The finite-difference step size used in all calculations is 5.0×10^{-4} bohrs, in combination with a DIIS convergence tolerance of 1.0×10^{-8} a.u. This step size has been shown to be robust and effective to a high level of accuracy in calculations of the DBOC,[33,38] and we find that this is also the case for the Berry curvature, with step sizes between 1.0×10^{-3} and 1.0×10^{-4} bohr, giving comparable results in most instances.

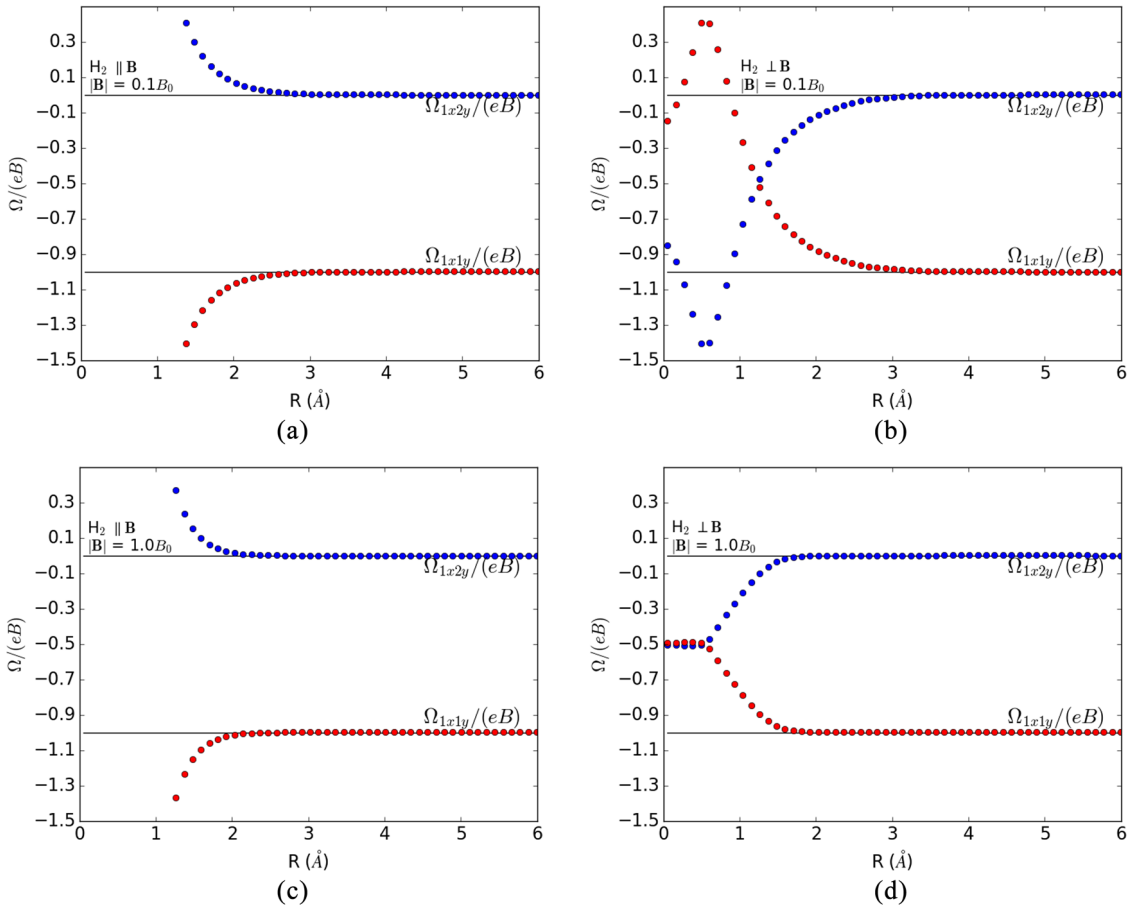

FIG. 6. Berry curvature of H_2 for the UHF $\beta\beta$ triplet state calculated with the u-cc-pVDZ basis set for orientations parallel [(a) and (c)] and perpendicular [(b) and (d)] to the magnetic field. The field is oriented along the *z*-axis with strengths of $|\mathbf{B}| = 0.1B_0$ [(a) and (b)] and $|\mathbf{B}| = 1.0B_0$ [(c) and (d)]. The molecular orientation perpendicular to the field is along the *x*-axis. The u-cc-pVDZ basis set is the decontracted cc-pVDZ basis.

For H_2 with the a uniform magnetic field along the z-axis and a molecular orientation either parallel or perpendicular to the field, the Berry curvature takes the form

$$\boldsymbol{\Omega}_{H_2} = \begin{pmatrix} \boldsymbol{\Omega}_{11} & \boldsymbol{\Omega}_{12} \\ \boldsymbol{\Omega}_{21} & \boldsymbol{\Omega}_{22} \end{pmatrix} = \left(\begin{array}{ccc|ccc} 0 & -\kappa & 0 & 0 & -\tau & 0 \\ \kappa & 0 & 0 & \tau & 0 & 0 \\ 0 & 0 & 0 & 0 & 0 & 0 \\ \hline 0 & -\tau & 0 & 0 & -\kappa & 0 \\ \tau & 0 & 0 & \kappa & 0 & 0 \\ 0 & 0 & 0 & 0 & 0 & 0 \end{array}\right) \tag{87}$$

where $\boldsymbol{\Omega}_{11} = \boldsymbol{\Omega}_{22}$ and $\boldsymbol{\Omega}_{12} = -\boldsymbol{\Omega}_{21}^{\mathrm{T}} = \boldsymbol{\Omega}_{21}$ and κ and τ are obtained from Eq. (49). Since in this particular case, all blocks are anti-symmetric, we may, as discussed in Sec. II G, calculate the Berry force in cross-product form using

$$\boldsymbol{\omega}_{11}^{\mathrm{A}} = \boldsymbol{\omega}_{22}^{\mathrm{A}} = \begin{pmatrix} 0 \\ 0 \\ \kappa \end{pmatrix}, \quad \boldsymbol{\omega}_{12}^{\mathrm{A}} = \boldsymbol{\omega}_{21}^{\mathrm{A}} = \begin{pmatrix} 0 \\ 0 \\ \tau \end{pmatrix}, \tag{88}$$

yielding the equations of motion

$$M_I \ddot{\overline{\mathbf{R}}}_I = \mathbf{F}_I^{\mathrm{BO}} - \sum_J \left(e\delta_{IJ} Z_I \mathbf{B} - \boldsymbol{\omega}_{IJ}^{\mathrm{A}} \right) \times \dot{\overline{\mathbf{R}}}_J. \tag{89}$$

Introducing screening charges Q_{IJ} as given in Eq. (68), we obtain

$$Q_{II} = -\frac{\kappa}{eB_z}, \quad Q_{IJ} = -\frac{\tau}{eB_z}, \tag{90}$$

and the equations of motion take the form

$$M_I \ddot{\overline{\mathbf{R}}}_I = \mathbf{F}_I^{\mathrm{BO}} - \sum_J e(\delta_{IJ} Z_I + Q_{IJ}) \mathbf{B} \times \dot{\overline{\mathbf{R}}}_J, \tag{91}$$

where the screening charges add up to the partial charge on each atom,

$$q_I = \sum_J Q_{IJ} = \sum_J Q_{JI}. \tag{92}$$

In general, however, the symmetric part of the Berry curvature does not vanish, and we cannot express the force in terms of screening charges.

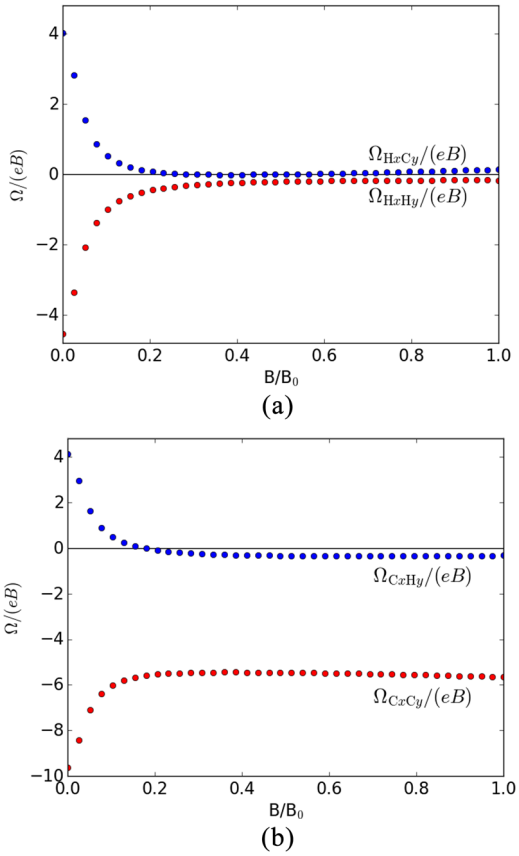

FIG. 7. Berry curvature of CH^+ for the RHF singlet state calculated with the cc-pVDZ basis set as a function of magnetic field strength. The magnetic field is oriented along the z-axis with the CH^+ molecule oriented perpendicular to the field along the x-axis. (a) HH and HC block elements and (b) CC and CH block elements. The bond distance is the zero-field equilibrium value of 1.1226 Å. The range of magnetic field strengths is $|\mathbf{B}| = 10^{-4}B_0$ to $|\mathbf{B}| = B_0$.

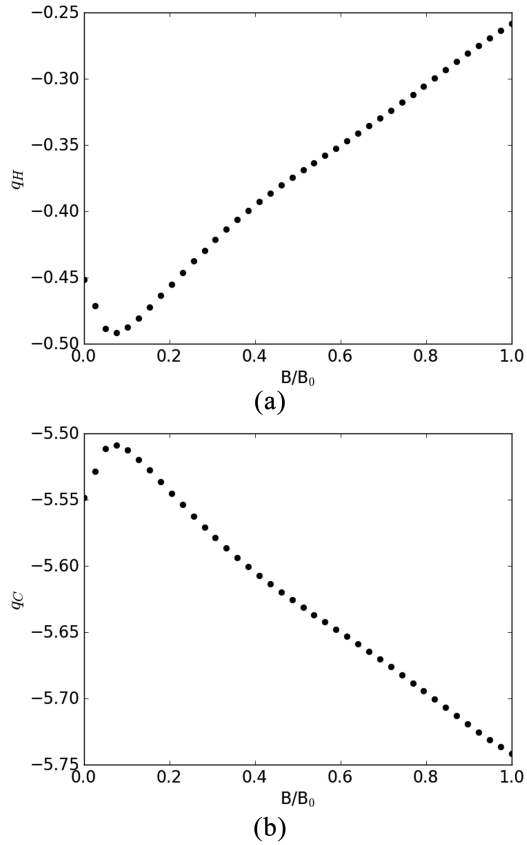

FIG. 8. Partial electronic charge for hydrogen q_H (a) and carbon q_C (b) calculated from Berry curvature elements for the RHF singlet state with the cc-pVDZ basis set as a function of magnetic field strength. The magnetic field is oriented along the z-axis with the CH^+ molecule oriented perpendicular to the field along the x-axis. The bond distance is the zero field equilibrium value of 1.1226 Å. The range of magnetic field strengths is $|\mathbf{B}| = 10^{-4}B_0$ to $|\mathbf{B}| = B_0$.

Our equations of motion for H_2 agree with those in Ref. 12, which are specialized to the case of the vanishing symmetric component of the Berry curvature. The definition in Ref. 12 of the Berry curvature corresponds to

$$\Omega_{\alpha}^{(IJ)} = -2\hbar\,\mathrm{Im}\big(\epsilon_{\alpha\beta\gamma}\langle\nabla_{I\beta}\phi|\nabla_{J\gamma}\phi\rangle\big) = \epsilon_{\alpha\beta\gamma}\Omega^{A}_{I\beta J\gamma}, \tag{93}$$

and hence, $\boldsymbol{\Omega}^{(IJ)} = -2\boldsymbol{\omega}^{\mathrm{A}}_{IJ}$. Their (anti-symmetric) Berry curvature thus differs from ours by a sign convention and a mistaken factor of two.

In Fig. 2, we have, for the singlet ground state of H_2 at the RHF/STO-3G level of theory plotted, the independent elements of the Berry curvature

$$\Omega_{1x1y} = -\kappa, \quad \Omega_{1x2y} = -\tau \tag{94}$$

as a function of the bond distance for field strengths of $0.1B_0$ and $1.0B_0$, with the magnetic field oriented along the z-axis and the molecule oriented either parallel or perpendicular to the field. These plots are in good agreement with the top panels in Fig. 1 of Ref. 12, although a change in the curvature moving from $0.1B_0$ to $1.0B_0$ is noted as the stronger field begins to compress the molecule. For magnetic field strengths ranging from the weak field to about $0.1B_0$, the values of $\Omega/|\mathbf{B}|$ do not vary appreciably as a function of bond distance for the STO-3G RHF case.

At very short bond distances, the calculated values of the Berry curvature are sensitive to the basis set. In particular, at bond distances less than 0.3 Å, the convergence to the zero bond-distance limit is not the same across the STO-3G, cc-pVDZ, and cc-pVTZ basis sets. While the STO-3G basis set converges to a value of $-0.5eB_0$ for both Ω_{1x1y} and Ω_{1x2y}, this behavior is not exhibited by the cc-pVDZ or the cc-pVTZ basis set, depending on the orientation to the field. Decontraction of the cc-pVDZ and cc-pVTZ basis sets greatly altered the convergence behavior in the region of small bond distance; see Fig. 3 for the cc-pVDZ basis set. Therefore, the decontracted basis sets, denoted u-cc-pVDZ and u-cc-pVTZ, have been used in subsequent Berry curvature calculations. Note that decontraction of the basis does not play a substantial

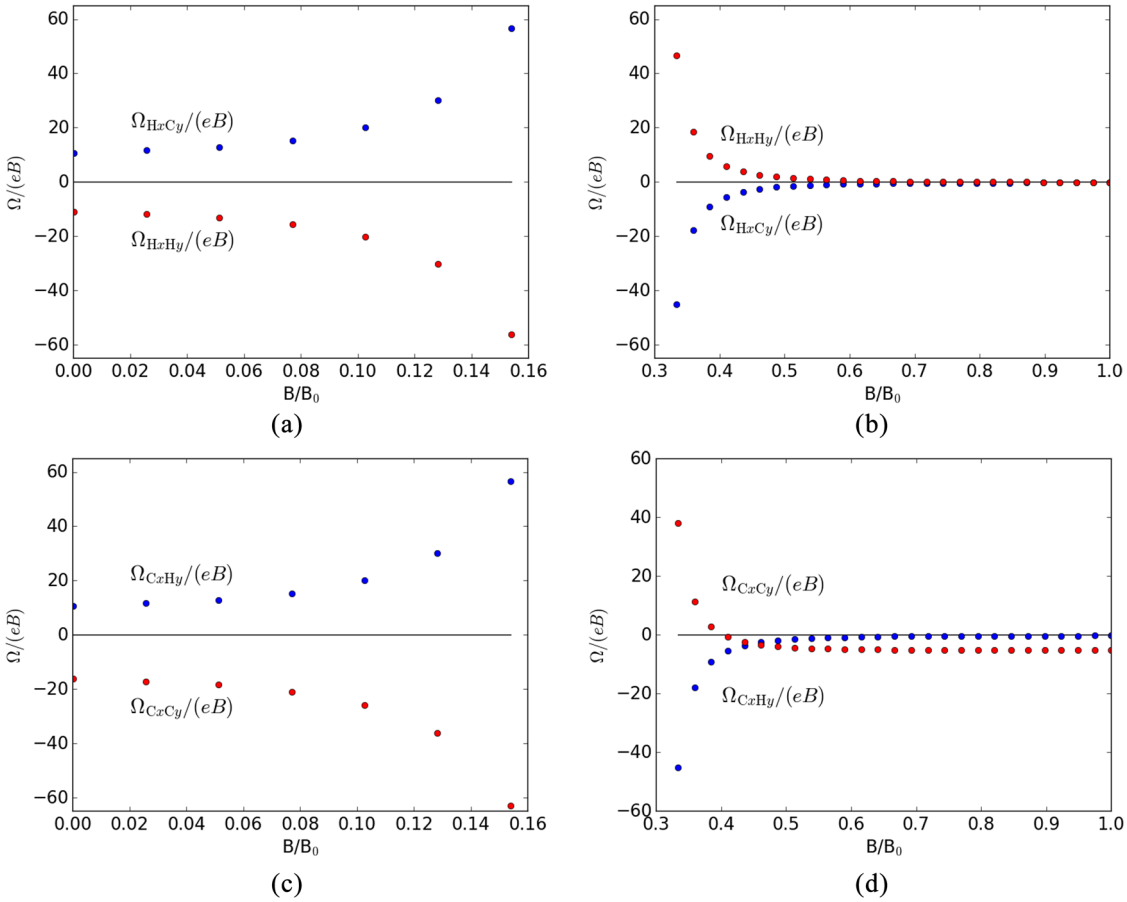

FIG. 9. Berry curvature of CH^+ for the RHF singlet state calculated with the cc-pVDZ basis set as a function of magnetic field strength. The magnetic field is oriented along the z-axis with the CH^+ molecule oriented parallel to the field along the z-axis. (a) and (b) HH and HC block elements and (c) and (d) CC and CH block elements. A level crossing occurs between $0.2B_0$ and $0.3B_0$, so data from this region were omitted in the plots. The bond distance is the zero field equilibrium value of 1.1226 Å. The range of magnetic field strengths is $|\mathbf{B}| = 10^{-4}B_0$ to $|\mathbf{B}| = B_0$.

role at larger internuclear separation, such as equilibrium, and the dissociation limit is the same for basis sets with or without contraction.

In Fig. 4, we have plotted the RHF/u-cc-pVDZ Berry curvature against the bond distance for the ground-state H_2 molecule at field strengths of $0.1B_0$ and $1.0B_0$. The trend exhibited by the STO-3G basis is also observed for the u-cc-pVDZ basis and for the u-cc-pVTZ basis as shown in the supplementary material. Antiscreening and superscreening effects are observed for the perpendicular orientation of H_2 across all basis sets, where at certain bond distances, the values of Ω_{1x2y} become positive (antiscreening) and the values of Ω_{1x1y} become less than $-1eB_0$ (superscreening). The reproduction of this trend across all basis sets and magnetic field strengths investigated here suggests it is not an artifact of the basis but a feature of the Berry curvature in this case.

Figures 5 and 6 show the Berry curvature of the $\beta\beta$ UHF triplet state in the STO-3G and u-cc-pVDZ basis sets, respectively. In the parallel orientation, the values of Ω_{1x2y} tend asymptotically from the antiscreening regime toward zero as the bond distance is increased, while the values of Ω_{1x1y} tend asymptotically from the superscreening regime toward $-1eB_0$. In the perpendicular orientation, the elements of the Berry curvature stay within the bounds of 0 and $-1eB_0$ for the STO-3G basis set. In the u-cc-pVDZ basis, Ω_{1x2y} and Ω_{1x1y} move into the antiscreening or superscreening regimes, depending on the field strength and bond distance. The same features are present in both Figs. 5 and 6, with the main differences being the magnitudes of the curvature, which vary depending on the field strength and basis set used.

Since the Berry curvature serves to screen the Lorentz force acting on the nuclei, it is noted that the elements Ω_{IxIy} and Ω_{IxJy} add up to the partial electronic charge associated with nucleus I. For H_2, this sum should be -1 for each nucleus, with the sum over both nuclei giving -2, indicating that the center of mass motion is completely screened as it should be in a neutral system. This is indeed what we observe in Figs. 2–6. Depending on the basis set and method, the values of Ω_{IxIy} and Ω_{IxJy} change as a function of bond distance, but their sum -1 is a constant.

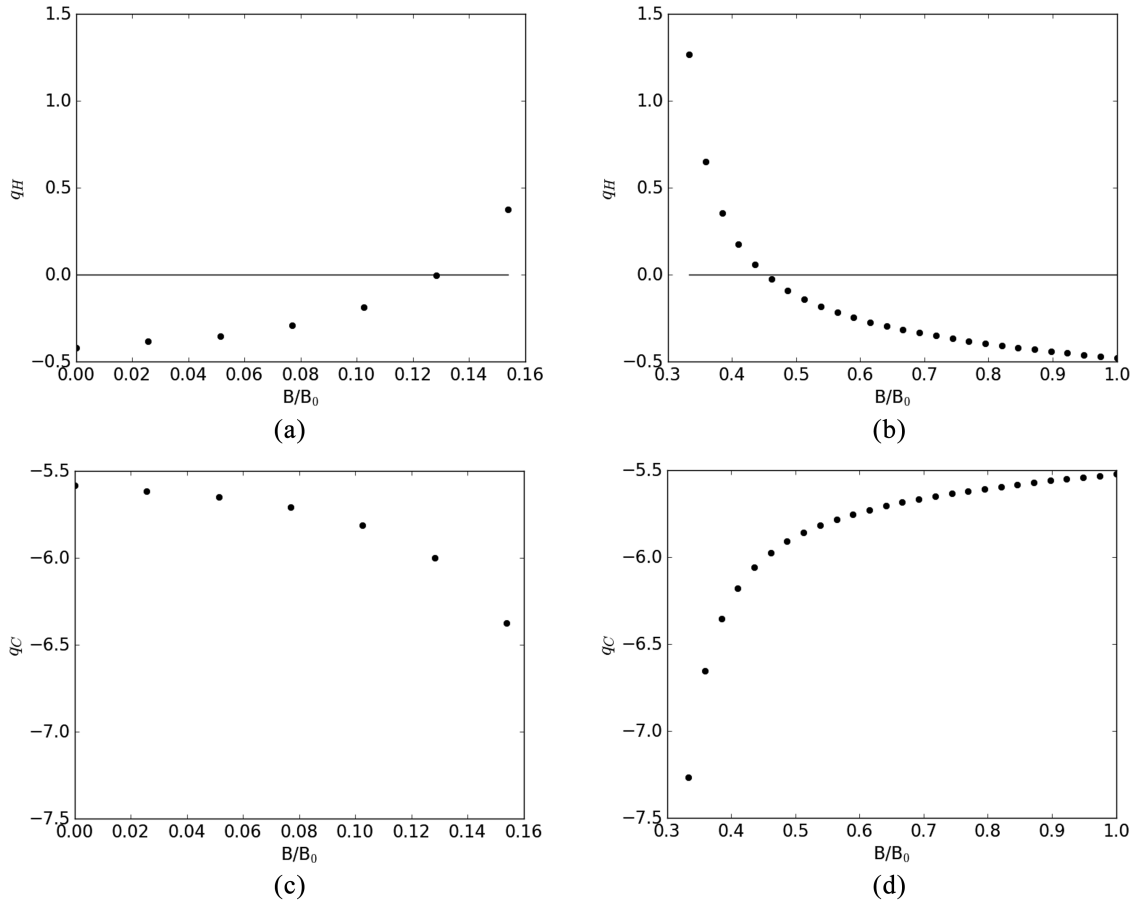

FIG. 10. Partial electronic charge for hydrogen q_H [(a) and (b)] and carbon q_C [(c) and (d)] calculated from Berry curvature elements for the RHF singlet state with the cc-pVDZ basis set as a function of magnetic field strength. The magnetic field is oriented along the z-axis with the CH^+ molecule oriented parallel to the field along the z-axis. A level crossing occurs in the region of $|\mathbf{B}| = 0.2B_0$ to $|\mathbf{B}| = 0.3B_0$, so data from this region were omitted in the plots. The bond distance is the zero field equilibrium value of 1.1226 Å. The range of magnetic field strengths is $|\mathbf{B}| = 10^{-4}B_0$ to $|\mathbf{B}| = B_0$.

C. CH^+ molecule

Berry-curvature values were calculated as a function of magnetic field strength in the range of $|\mathbf{B}| = 0.0001B_0$ to $|\mathbf{B}| = B_0$ for the CH^+ molecule using finite differences as outlined in Sec. II. Calculations were performed for the RHF singlet state with the cc-pVDZ basis set at the zero field equilibrium geometry of 1.1226 Å. The magnetic field was oriented along the z-axis, and calculations were performed both parallel and perpendicular to the magnetic field, with the perpendicular orientation of the molecule being specifically along the x-axis.

The Berry curvature tensor of CH^+ has a lower symmetry than that of H_2. For the parallel and perpendicular orientations of CH^+ to the magnetic field, the structure of the Berry curvature tensor is

$$\boldsymbol{\Omega} = \begin{pmatrix} \boldsymbol{\Omega}_{CC} & \boldsymbol{\Omega}_{CH} \\ \boldsymbol{\Omega}_{HC} & \boldsymbol{\Omega}_{HH} \end{pmatrix} = \begin{pmatrix} 0 & -\omega_{CC} & 0 & 0 & -\omega_{HC} & 0 \\ \omega_{CC} & 0 & 0 & \omega_{CH} & 0 & 0 \\ 0 & 0 & 0 & 0 & 0 & 0 \\ 0 & -\omega_{CH} & 0 & 0 & -\omega_{HH} & 0 \\ \omega_{HC} & 0 & 0 & \omega_{HH} & 0 & 0 \\ 0 & 0 & 0 & 0 & 0 & 0 \end{pmatrix}, \tag{95}$$

obeying the overall symmetry $\boldsymbol{\Omega}_{CH} = -\boldsymbol{\Omega}_{HC}^{T}$. However, since $\boldsymbol{\Omega}_{CH} \neq -\boldsymbol{\Omega}_{CH}^{T}$ and $\boldsymbol{\Omega}_{HC} \neq -\boldsymbol{\Omega}_{HC}^{T}$, the Berry force of CH^+ (unlike that of H_2) cannot be expressed in cross-product form. For interpretation purposes, we, nevertheless, calculate the partial charges of C and H from an average of ω_{CH}/ω_{HC} as follows:

$$q_C = Q_{CC} + Q_{CH} = -\frac{\omega_{CC}}{eB_z} - \frac{\omega_{CH} + \omega_{HC}}{2eB_z}, \tag{96}$$

$$q_H = Q_{HH} + Q_{HC} = -\frac{\omega_{HH}}{eB_z} - \frac{\omega_{HC} + \omega_{CH}}{2eB_z}. \tag{97}$$

For the perpendicular orientation of CH^+ to the magnetic field, Fig. 7 shows the values of the individual xy components for the hydrogen, carbon, and mixed blocks of the Berry curvature tensor plotted as a function of magnetic field strength. For each atom, the partial charge as a function of field strength is plotted in Fig. 8. The corresponding data for the parallel orientation are plotted in Figs. 9 and 10.

In the perpendicular case, it is seen from Fig. 8 that the charge is distributed unequally; moreover, the polarity of this distribution is enhanced as the field is increased. The electronic partial charge associated with the hydrogen nucleus tends toward zero as the field strength increases to $1.0B_0$, while the partial charge associated with the carbon nucleus tends toward −6. The magnitude of the sum of the two partial charges is always equal to the total number of electrons.

In the parallel case, a level crossing is observed in the region of magnetic field strengths of $0.2B_0$–$0.3B_0$. As such, the values of the Berry curvature tensor in this region are excluded from Figs. 9 and 10. The values of the partial charges given in Fig. 10 increase for hydrogen and decrease for carbon in the vicinity of the level crossing, but the values in the limit of weak fields and strong fields are very similar, in contrast with the perpendicular orientation.

IV. CONCLUSIONS

In this work, we have presented a general scheme for calculating the Berry curvature using finite differences. This was accomplished through a phase correction of each perturbed wave function in the finite-difference procedure, which results in a vanishing geometric vector potential. In the context of finite differences, such a correction is equivalent to the calculation of the derivatives in a consistent gauge. The scheme has been implemented in the program package LONDON,[15] which uses London atomic orbitals for gauge-origin invariant calculations of molecules in a magnetic field. It should be noted that, while we have reported on Hartree–Fock wave functions, the method is generally applicable and can be used in the cases of density functional theory (DFT) and functional configuration interaction (FCI), for example.

Basis-set studies on small atoms demonstrated that the reliability of the calculated Berry curvature depends critically on the use of London atomic orbitals—without London orbitals, the results are unreliable and the basis-set convergence is slow; with London orbitals, the convergence is rapid and a qualitatively correct Berry curvature is obtained even in a minimal basis.

The H_2 and CH^+ molecules were studied using London orbitals. The Berry curvature was calculated as a function of bond distance for H_2 at both the RHF and UHF levels of theory and as a function of magnetic field strength for CH^+ at the RHF level of theory. For short bond distances, less than 0.5 bohr, the behavior of the Berry curvature was found to be very sensitive to the basis set used. The H_2 results at the RHF/STO-3G level of theory agree with previous calculations of the Berry curvature for H_2 in a minimal London Slater basis.

The trends of the Berry curvature across multiple basis sets and field strengths were investigated. Berry antiscreening and superscreening were observed across multiple basis sets, indicating that these are real physical phenomena and not solely basis-set effects. For CH^+ in the perpendicular orientation, the polarity of the electronic partial charges on hydrogen and carbon increases with increasing field strength. In the parallel orientation, by contrast, the partial charges are roughly the same in the weak- and strong-field limits, with a level crossing occurring at intermediate field strengths.

The calculation of the Berry curvature from finite differences opens up the possibility of accurately calculating the screening force due to the electrons in *ab initio* molecular dynamics simulations. The screening of the Lorentz force is of crucial importance and can change the dynamics of atoms and molecules in a magnetic field qualitatively. Consequently, the calculation of the Berry curvature will be important for future work pertaining to molecular dynamics in magnetic fields.

SUPPLEMENTARY MATERIAL

See the supplementary material for Berry curvature plots with the cc-pVTZ basis set.

ACKNOWLEDGMENTS

We thank Laurenz Monzel, Ansgar Pausch, and Wim Klopper (Karlsruher Institut für Technologie) for helpful discussions. This work was supported by the Research Council of Norway through

"Magnetic Chemistry" (Grant No. 287950) and the CoE Hylleraas Center for Quantum Molecular Sciences (Grant No. 262695).

DATA AVAILABILITY

The data that support the findings of this study are available within the article and its supplementary material.

REFERENCES

[1]M. V. Berry, Proc. R. Soc. London, Ser. A **392**, 45 (1984).
[2]R. Resta, J. Phys.: Condens. Matter **12**, R107 (2000).
[3]J. W. Zwanziger, M. Koenig, and A. Pines, Annu. Rev. Phys. Chem. **41**, 601 (1990).
[4]D. J. Moore, Phys. Rep. **210**, 1 (1991).
[5]C. A. Mead, Rev. Mod. Phys. **64**, 51 (1992).
[6]D. Marx and J. Hutter, *Ab Initio Molecular Dynamics: Basic Theory and Advanced Methods* (Cambridge University Press, 2009).
[7]F. F. D. Carvalho, M. E. Bouduban, B. F. Curchod, and I. Tavernelli, Entropy **16**, 62 (2014).
[8]M. Born and R. Oppenheimer, Ann. Phys. **389**, 457 (1927).
[9]G. Hunter, Int. J. Quantum Chem. **9**, 237 (1975).
[10]A. Abedi, N. T. Maitra, and E. K. U. Gross, Phys. Rev. Lett. **105**, 123002 (2010).
[11]R. Requist, F. Tandetzky, and E. K. U. Gross, Phys. Rev. A **93**, 042108 (2016).
[12]D. Ceresoli, R. Marchetti, and E. Tosatti, Phys. Rev. B: Condens. Matter Mater. Phys. **75**, 161101 (2007); arXiv:0703551 [cond-mat].
[13]P. Schmelcher, L. S. Cederbaum, and H.-D. Meyer, Phys. Rev. A **38**, 6066 (1988).
[14]T. Detmer, P. Schmelcher, and L. S. Cederbaum, J. Phys. B: At., Mol. Opt. Phys. **28**, 2903 (1995).
[15]E. Tellgren, T. Helgaker, A. Soncini, K. K. Lange, A. M. Teale, U. Ekström, S. Stopkowicz, J. H. Austad, and S. Sen, "LONDON: A quantum-chemistry program for plane-wave/GTO hybrid basis sets and finite magnetic field calculations," see londonprogram.org for more information.
[16]F. London, J. Phys. Radium **8**, 397 (1937).
[17]H. F. Hameka, Mol. Phys. **1**, 203 (1958).
[18]R. Ditchfield, J. Chem. Phys. **65**, 3123 (1976).
[19]T. Helgaker and P. Jørgensen, J. Chem. Phys. **95**, 2595 (1991).
[20]E. I. Tellgren, A. Soncini, and T. Helgaker, J. Chem. Phys. **129**, 154114 (2008).
[21]E. I. Tellgren, S. S. Reine, and T. Helgaker, Phys. Chem. Chem. Phys. **14**, 9492 (2012).
[22]T. J. P. Irons, J. Zemen, and A. M. Teale, J. Chem. Theory Comput. **13**, 3636 (2017).
[23]A. Pausch and W. Klopper, Mol. Phys. **118**, e1736675 (2020).
[24]E. I. Tellgren, T. Helgaker, and A. Soncini, Phys. Chem. Chem. Phys. **11**, 5489 (2009).
[25]E. I. Tellgren, A. M. Teale, J. W. Furness, K. K. Lange, U. Ekström, and T. Helgaker, J. Chem. Phys. **140**, 034101 (2014).
[26]J. W. Furness, J. Verbeke, E. I. Tellgren, S. Stopkowicz, U. Ekström, T. Helgaker, and A. M. Teale, J. Chem. Theory Comput. **11**, 4169 (2015).
[27]K. K. Lange, E. I. Tellgren, M. R. Hoffmann, and T. Helgaker, Science **337**, 327 (2012).
[28]J. Austad, A. Borgoo, E. I. Tellgren, and T. Helgaker, Phys. Chem. Chem. Phys. **22**, 23502 (2020); arXiv:2005.04638.
[29](a) S. Stopkowicz, J. Gauss, K. K. Lange, E. I. Tellgren, and T. Helgaker, J. Chem. Phys. **143**, 074110 (2015); arXiv:1505.08045; (b) F. Hampe and S. Stopkowicz, *ibid.* **146**, 154105 (2017); (c) J. Chem. Theory Comput. **15**, 4036–4043 (2019); (d) F. Hampe, N. Gross, and S. Stopkowicz, Phys. Chem. Chem. Phys. **22**, 23522–23529 (2020).
[30]S. Sen, K. K. Lange, and E. I. Tellgren, J. Chem. Theory Comput. **15**, 3974 (2019).
[31]N. C. Handy, Y. Yamaguchi, and H. F. Schaefer, J. Chem. Phys. **84**, 4481 (1986).
[32]A. G. Ioannou, R. D. Amos, and N. C. Handy, Chem. Phys. Lett. **251**, 52 (1996).
[33]E. F. Valeev and C. D. Sherrill, J. Chem. Phys. **118**, 3921 (2003).
[34]D. Ceresoli and E. Tosatti, Phys. Rev. Lett. **89**, 116402 (2002).
[35]J. I. Rawlinson and C. Tronci, Phys. Rev. A **102**, 032811 (2020).
[36]J. C. Tully, J. Chem. Phys. **93**, 1061 (1990).
[37]J. E. Subotnik, A. Jain, B. Landry, A. Petit, W. Ouyang, and N. Bellonzi, Annu. Rev. Phys. Chem. **67**, 387 (2016).
[38]W. Cencek and W. Kutzelnigg, Chem. Phys. Lett. **266**, 383 (1997).
[39]P. E. Schneider, F. Pavošević, and S. Hammes-Schiffer, J. Phys. Chem. Lett. **10**, 4639 (2019).
[40]T. H. Dunning, J. Chem. Phys. **90**, 1007 (1989).
[41]R. A. Kendall, T. H. Dunning, Jr., and R. J. Harrison, J. Chem. Phys. **96**, 6796 (1992).
[42]W. J. Hehre, R. F. Stewart, and J. A. Pople, J. Chem. Phys. **51**, 2657 (1969).